Journal of Inflammation Research Dovepress

Open Access Full Text Article ORIGINAL RESEARCH

The METTL3/m6A Reader Protein YTHDF1 Regulates Endothelial Cell Pyroptosis by Enhancing NLRP3 Expression to Affect Soft Tissue Injury

Xuesong Xie[1], Fang Fang[2]

[1]Department of Orthopedics, Xiangtan Central Hospital, Xiangtan, 411100, People's Republic of China; [2]Department of Anorectal, Xiangtan Central Hospital, Xiangtan, 411100, People's Republic of China

Correspondence: Fang Fang, Email 13607493657@163.com

Background: Pyroptosis is inflammation-associated programmed cell death triggered by activation of the NOD-like receptor protein 3 (NLRP3) inflammasome, which plays a crucial role in acute soft tissue injury (ASTI). This study aimed to explore whether methyltransferase-like 3 (METTL3) can regulate NLRP3 expression through N6-methyladenosine (m6A) modification to mediate endothelial cell pyroptosis and thus affect soft tissue injury.

Methods: An experimental ASTI rat model was created by inducing muscle injury through striking the rat muscle. In vitro, an ASTI cell model was established using human umbilical vein endothelial cells (HUVECs) stimulated with lipopolysaccharide (LPS) and ATP. The severity of ASTI in rats was evaluated using H&E staining. To assess protein levels, Western blot and Immunohistochemistry (IHC) analyses were performed, focusing on METTL3, pyroptosis-associated proteins, and m6A reader proteins. Immunofluorescence (IF) assay was conducted to examine the expression of NLRP3 and CD31. The levels of inflammatory cytokines were measured using an ELISA assay, while flow cytometry was used to detect levels of ROS and cellular pyroptosis. The m6A levels in cells were analyzed by RNA m6A colorimetry. The interactions between METTL3 and NLRP3, and YTHDF1 and NLRP3 were analyzed using RIP and RNA pull-down assays, respectively.

Results: METTL3 and YTHDF1 were significantly upregulated in ASTI rats and LPS-ATP-induced HUVECs. Knockdown of METTL3 ameliorated ASTI and inhibited cellular pyroptosis. Knockdown of METTL3 reduced the levels of total m6A and NLRP3 m6A in HUVECs and suppressed NLRP3 expression. Meanwhile, knockdown of YTHDF1 decreased NLRP3 protein expression without affecting NLRP3 mRNA levels. In addition, overexpression of NLRP3 was able to reverse the effect of METTL3 on LPS-ATP-induced endothelial cell pyroptosis.

Conclusion: The METTL3/m6A reader protein YTHDF1 regulates endothelial cell pyroptosis by enhancing NLRP3 expression to affect soft tissue injury.

Keywords: acute soft tissue injury, ASTI, cell pyroptosis, METTL3, m6A modification, YTHDF1, NLRP3

Introduction

Acute soft tissue injury (ASTI), a prevalent sports injury with substantial implications for individuals' well-being and productivity, has attracted growing attention in the clinical field.[1] Injuries can manifest themselves in a variety of ways, including localized edema, muscle fiber rupture, pain, bruising, ecchymosis, and dysfunction.[2] Following soft tissue injury, the body repairs the damage through an inflammatory response.[3] This process involves the aggregation of immune cells and functional changes in endothelial cells. Research indicates that the dysfunction of endothelial cells plays a role in the occurrence and advancement of certain soft tissue injuries such as muscle atrophy.[4,5] Therefore, exploring ways to reduce inflammation-induced endothelial cell damage is important for the treatment of ASTI.

Received: 21 May 2024
Accepted: 10 December 2024
Published: 20 December 2024

Cell pyroptosis is a type of programmed cell death characterized by intense inflammation. It differs from apoptosis and necrosis and is triggered by the activation of a protein called NOD-like receptor protein 3 (NLRP3) inflammasome.[6] This activation leads to the conversion of cytokine precursors, pro-IL-1β and pro-IL-18, into active cytokines by pro-Caspase-1 (after cleavage by the NLRP3 inflammasome).[7,8] Additionally, Caspase-1 can produce the N-terminal fragment of GSDMD (GSDMD-N), which then forms pores on the cell membrane and induces pyroptosis.[9,10] Immediately after the formation of GSDMD pores, cells die and large quantities of IL-1β and IL-18 are released from the GSDMD pores, resulting in a cascade of inflammatory responses.[11] Although recent studies have reported that inhibition of endothelial cell pyroptosis promotes wound healing,[12] the link between NLRP3 inflammatory vesicles and ASTI is unclear.

Methyltransferase-like 3 (METTL3) is a protein that acts as an RNA methyltransferase and plays a role in various processes related to mRNA, including biogenesis, decay, and translational control. It achieves these functions through a specific modification known as N6-methyladenosine (m6A) on RNA molecules.[13] The m6A modification is a common and important RNA modification found in eukaryotes. It plays a crucial role in regulating essential biological processes, including gene expression control and the maintenance of mRNA stability and balance.[14] Extensive research has shown that m6A modification exerts a substantial influence on wound healing by modulating the expression of genes involved in crucial cellular processes.[15] For example, ADSCs promote diabetic foot ulcer wound healing by enhancing VEGF3-mediated lymphangiogenesis through METTL3-mediated modification of VEGF-C m6A.[16] The presence of METTL3 promotes m6A modification on the mRNA of NLRP3, leading to increased stability of the NLRP3 mRNA. This, in turn, enhances the interaction between ZBP1 and NLRP3 proteins, ultimately facilitating trophoblast cell pyroptosis.[17] However, whether METTL3 affects endothelial cell pyroptosis in ASTI by mediating NLRP3 m6A modification has not been investigated.

In this study, our main objective was to examine the role of METTL3 in regulating NLRP3 expression through m6A modification, which in turn influences endothelial cell pyroptosis and ultimately affects ASTI. By uncovering these mechanisms, our findings have the potential to aid in the identification of therapeutic targets for the treatment of ASTI.

Methods and Materials

Animals and Treatments

Male SD rats (6–8 weeks old, Hunan Slake Jinda Laboratory Animal Center, Changsha, China) were acclimatized and fed for 1 week. Before modeling, rats were anesthetized with 2% sodium pentobarbital, and then the hair on the right hind leg was removed. According to a previous report, an ASTI model was established, in which a 200 g weight was dropped from a height of 50 cm and impacted the middle calf muscle of rats 10 times in a row (the impact area was about 2 cm^2).[18] Swelling and subcutaneous ecchymosis visible at the impact site indicated successful modeling. Only plucked anesthetized rats were used as the Sham group. Rats in the LV-NC or LV-sh-METTL3 group were injected with a single dose of 1×10^8 TU LV-NC or LV-sh-METTL3 (HG-HR001024794, Honorgene, Changsha, China), respectively, via the tail vein one week before modeling (n=6).[19] After 7 days of modeling, the rats were euthanized. Muscle tissues from the injured area were then collected for further analysis.

H&E Staining

Rat muscle tissues were collected and fixed using 4% paraformaldehyde. The collected tissues were fixed and subsequently embedded in paraffin. Following this, tissue sections were prepared and stained using a combination of hematoxylin (AWI0001a, Abiowell, Changsha, China) and eosin (AWI0029a, Abiowell) stains. The stained sections were covered with a layer of neutral gum and subsequently examined using a light microscope (BA210T, Motic, Xiamen, China) for further observation.

Cells Culture and Treatments

Human umbilical vein endothelial cells (HUVECs, BH-C277, Bohui Biotechnology Co., Ltd, Guangzhou, China) were cultured in endothelial cell medium (ECM) and then cultured at 37°C with 5% CO_2. An in vitro injury model was

prepared using the lipopolysaccharide (LPS)-ATP method.[12] In the experimental setup, HUVECs were initially cultured in a serum-free medium. To induce inflammation, the cells were treated with LPS (1 μg/mL, S1732, Beyotime, Shanghai, China) for 6 h. After that, the cells were further stimulated with ATP (5 mm, D7378, Beyotime) for 30 min. The Control group consisted of cells cultured without any exposure or treatment. The Model group comprised cells induced by LPS-ATP stimulation. LPS-ATP-induced cells were transfected with sh-NC, sh-METTL3, and sh-YTHDF1 to form the sh-NC, sh-METTL3, and sh-YTHDF1 groups, respectively. The sh-METTL3+oe-NC group consisted of cells induced by LPS-ATP and transfected with both sh-METTL3 and oe-NC. Finally, the sh-METTL3+oe-NLRP3 group comprised cells induced by LPS-ATP and transfected with sh-METTL3 and oe-NLRP3 (overexpressed-NLRP3). The sh-NC, sh-METTL3 (HG-HS019852), sh-YTHDF1 (HG-HS001031732), oe-NC, and oe-NLRP3 (HG-HO001243133) were designed and purchased from Honorgene.

Western Blot

Rat muscle tissues or HUVECs were lysed using RIPA buffer (AWB0136, Abiowell). The protein content was analyzed using the BCA Protein Quantification Kit (23227, Thermo fisher). Protein was then separated on a 10% SDS-PAGE gel using gel electrophoresis and subsequently transferred onto nitrocellulose membranes. To block the membranes, 5% skim milk powder in 1×PBST was prepared and the membranes were immersed in this solution. The membranes were then incubated with the primary antibody overnight at 4°C. Primary antibodies included METTL3 (1:1000, ab195352, Abcam, Cambridge, UK), NLRP3 (AWA46822, 1:1000, Abiowell), Cleaved-Caspase-1 (AWA44820, 1:1000, Abiowell), IL-1β (AWA46641, 1:1000, Abiowell), IL-18 (AWA49529, 1:1000, Abiowell), GSDMD-N (1:1000, ab215203, Abcam), GSDMD (1:5000, 20770-1-AP, Proteintech, Chicago, USA), YTHDF1 (AWA53935, 1:1000, Abiowell), YTHDF2 (AWA57692, 1:1000, Abiowell), YTHDF3 (AWA50880, 1:1000, Abiowell), IGF2BP1 (Ab290736, 1:1000, Abcam), IGF2BP2 (AWA57873, 1:1000, Abiowell), IGF2BP3 (AWA00010, 1:1000, Abiowell), GAPDH (1:5000, AWA80007, Abiowell), and β-actin (1:5000, AWA80002, Abiowell). Then incubation with goat anti-rabbit IgG (SA00001-2, 1:6000, Proteintech) or goat anti-mouse IgG (SA00001-1, 1:5000, Proteintech) secondary antibody. The protein bands were measured by incubating with ECL chemiluminescent solution (AWB0005, Abiowell) for 1 min, then imaged in the imaging system.

Immunohistochemistry (IHC)

The rat muscle tissue slices were subjected to dewaxing using xylene and then rehydrated through a series of ethanol concentrations. Following this, tissue slices were placed in a 0.01 M citrate buffer (pH 6.0) and heated to a boiling point. The heating was then maintained for an additional 20 min before cooling down and rinsing with PBS. Subsequently, the slices were treated with 1% periodate for 10 min. The slices were incubated with appropriate primary antibodies: METTL3 (AWA50965, 1:200, Abiowell), NLRP3 (AWA46822, 1:200, Abiowell), and GSDMD-N (AWA55860, 1:200, Abiowell) overnight at 4 °C, followed by incubation with goat anti-rabbit IgG H&L (31460, Invitrogen, Carlsbad, USA) at 37°C for 30 min. DAB (ZLI-9018, Beijing Zhongsui Jinqiao Biotechnology Co., Beijing, China) and hematoxylin (AWI0001a, Abiowell) were used for color development and nuclear staining, respectively.

Immunofluorescence (IF)

The rat muscle tissue slices were subjected to dewaxing using xylene and then rehydrated through a series of ethanol concentrations. Following this, the tissue slices were immersed in a 0.01 M citrate buffer with a pH of 6.0, heated to boiling, then the heating was stopped and the sections were boiled continuously for 20 min, cooled, and washed with PBS. The slices were placed in sodium borohydride solution, and treated using 0.3% H_2O_2 for 15 min. Next, they were blocked using 5% BSA for 60 min. Afterwards, the slices were incubated overnight at 4°C with primary antibodies specific for CD31 (AWA58016, 1:100, Abiowell) and NLRP3 (AWA46822, 1:100, Abiowell). Following this, the slices were incubated with goat anti-rabbit secondary antibody (31460, Invitrogen) at 37°C for 30 min. Additionally, the slices were incubated with TYP-570 fluorescent dye for 5 min at 37°C. To visualize the nuclei, DAPI staining was employed.

Elisa

Collected blood samples and cells were centrifuged at 1000 g for 15 min to obtain serum and cell supernatant. We measured the levels of inflammatory factors IL-1β and IL-18 by using ELISA in accordance with the protocols from specialized commercial kits: human (CSB-E08053h) and rat (CSB-E08055r) IL-1β ELISA Kits, human (CSB-E07450h) and rat (CSB-E04610r) IL-18 ELISA Kits. These kits were purchased from Cusabio, Wuhan, China.

Detection of ROS

ROS production in rat muscle tissues or HUVECs was measured by using ROS Assay Kit (S0033S, Beyotime), the procedures followed the manufacturer's protocols. The ROS levels were analyzed using a flow cytometer (a00-1-1102, Beckman, Pasadena, USA).

Detection of Cell Pyroptosis

To obtain a cell suspension, the HUVECs were treated with 0.25% trypsin. We measured cell pyroptosis by using FAM-FLICA® Caspase-1 YVAD Assay Kit (ICT-97, ImmunoChemistry, Davis, USA). The treated cells were added with FAM-YVAD-FMK and then stained with PI for 60 min. The levels of pyroptosis in the cells were analyzed using a flow cytometer (a00-1-1102, Beckman).

RNA m6A Colorimetric Assay

We evaluated the levels of m6A RNA methylation in HUVECs by using the m6A RNA Methylation Quantification Kit (Colorimetric) (Ab185912, Abcam). The procedures followed the manufacturer's protocols.

RIP Assay

For RIP analysis, we used the Imprint® RIP Kit (RIP, Sigma-Aldrich, St. Louis, USA) as per the manufacturer's instructions. Initially, magnetic beads coated with 5 μg of specific antibodies targeting m6A (68055-1-Ig, Proteintech) were incubated with the prepared RIP Immunoprecipitation Buffer overnight at 4°C. Following this, the complex was treated with a protease K digestion. To extract the RNA, we employed the phenol-chloroform method. Following extraction, the relative interaction between m6A and NLRP3 transcripts was assessed using RT-qPCR.

RT-qPCR

RNA was extracted from HUVECs using Trizol (15596026, Thermo fisher), and then the mRNA was reversed to cDNA using the mRNA Reverse Transcription Kit (CW2569, CWBIO, Beijing, China). 2 μL of cDNA was added into mix solution containing 15 μL of 2×SYBGREEN PCR Master Mix (CW2601, CWBIO), and 1 μL specific primer for RT-qPCR detection. The primer sequences used for RT-qPCR can be found in Table 1.

RNA Pull-Down Assay

We employed the Pierce™ Magnetic RNA-Protein Pull-Down Kit (20164, Thermo fisher, Rockford, USA) following the manufacturer's instructions. In brief, 50 pmol of biotinylated RNA was combined with 2 mg of protein lysate and 50 μL of magnetic streptavidin beads. The mixture was then incubated and subsequently washed three times to remove non-specific binding. The streptavidin beads were then boiled, and the resulting eluate was used for Western blot analysis to

Table 1 Primer Sequences Were Used in This Study

Name	Sequences (5'-3')
β-actin	F- ACCCTGAAGTACCCCATCGAG
	R- AGCACAGCCTGGATAGCAAC
NLRP3	F- GCCACGCTAATGATCGACT
	R- TCTTCCTGGCATATCACAGT

detect the proteins that specifically interacted with the biotinylated RNA. Primary antibodies used in this experiment included YTHDF1 (17479-1-AP, 1:1000, Proteintech). HRP-labeled goat anti-rabbit IgG (H+L) (AWS0002, 1:5000, Abiowell) was used as secondary antibody.

Statistical Analysis

All collected data were analyzed using GraphPad Prism 9 software. The results are depicted as mean values with corresponding standard deviations. To assess the statistical significance between the two groups, the Student's *t*-test was used. For analyses involving multiple groups, either one-way ANOVA or two-way ANOVA was conducted. A p-value < 0.05 was considered to indicate statistical significance.

Results

Expression Pattern of m6A Methyltransferase in ASTI Rats

We verified whether the ASTI rat models were constructed successfully by examining the muscle surface of the rats as well as H&E staining of the muscle tissue sections. Figure 1A showed that there was no hemorrhage, bruising, or edema in the rats of the Sham group, whereas the rats of the ASTI group showed severe hemorrhage, bruising, and edema. Subsequently, H&E staining was used to observe the histological changes and cellular infiltration in the muscle tissue sections of the rats. The Sham group had normal muscle fiber arrangement and muscle cell shape. However, the ASTI group had a severe inflammatory response in the soft tissues, accompanied by significant inflammatory cell infiltration, muscle fiber breakage, swelling, widening of the intermuscular septum, and muscle fiber degeneration (Figure 1B). These results indicated that ASTI rat models were constructed successfully. m6A methyltransferases mainly includes METTL3, METTL14, and WTAP.[20] We examined the protein levels of these three m6A methyltransferases in rat muscle tissues. The results revealed that in the ASTI group of rats, the expression levels of METTL3, METTL14, and WTAP were significantly increased compared to the Sham group. Notably, the expression of METTL3 showed the most pronounced difference between the two groups (Figure 1C). Furthermore, IHC results of rat muscle tissues also showed that METTL3 levels were significantly higher in rats of the ASTI group than in the Sham group (Figure 1D). Therefore, we concluded that METTL3 was a key factor affecting ASTI.

Modulation of METTL3 Affects ASTI and Cell Pyroptosis in ASTI Rats

To further examine the effects of METTL3 on ASTI and cell pyroptosis, we knocked down METTL3 in rats using lentivirus carrying sh-METTL3. The muscle surface of the rats as well as H&E staining of the muscle tissue sections showed a significant alleviation of the symptoms of ASTI in ASTI rats knocked down with METTL3 (Figure 2A and B). The Western blot analysis in Figure 2C confirmed that the expression of METTL3 was decreased in rats that were transfected with the sh-METTL3 lentivirus. It is known that endothelial cell pyroptosis plays a significant role in the healing of wounds,[12] and it may also have an impact on ASTI. Therefore, we investigated whether cell pyroptosis is involved in ASTI and examined the role of METTL3 in this process by assessing the activation of the NLRP3 inflammasome in rats with ASTI. Western blot results revealed a significant increase in protein levels of pyroptosis-related proteins in the ASTI group compared to the Sham group. Conversely, in the LV-sh-METTL3 group, there was a notable decrease in the levels of these pyroptosis-related proteins compared to the LV-NC group (Figure 2D). In addition, IHC detection of NLRP3 and GSDMD-N showed similar changes (Figure 2E). We used NLRP3/CD31 double staining to further analyze endothelial cell pyroptosis in damaged muscle tissues. The IF results showed an increased number of co-localized NLRP3 and CD31 in the ASTI group compared to the Sham group, indicating more NLRP3-positive endothelial cells, whereas knockdown of METTL3 resulted in fewer NLRP3-positive endothelial cells (Figure 2F). As shown in Figure 2G, the levels of IL-1β and IL-18 were notably elevated in the ASTI group in comparison to the Sham group. However, the knockdown of METTL3 resulted in a significant reduction in the levels of IL-1β and IL-18. Additionally, since the production of ROS is known to play a crucial role in the activation of the NLRP3 inflammasome,[21] we further investigated the levels of ROS in the muscle tissues of rats in each group. The findings showed that there was an increase in levels of ROS in rats of the ASTI group compared to the Sham group.

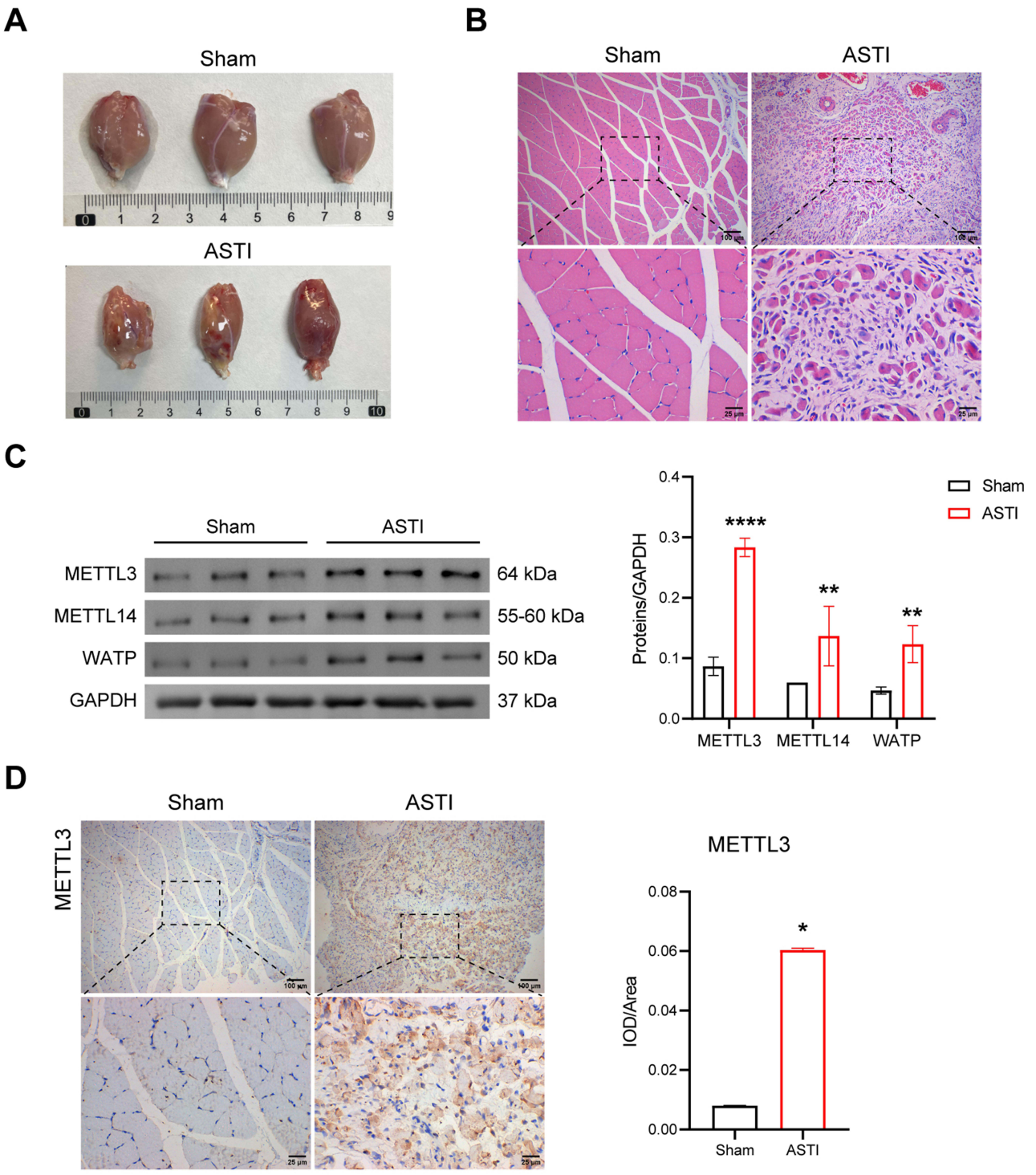

Figure 1 Expression pattern of m6A methyltransferase in ASTI rats. (**A**) The images of the surface of muscle from rats. (**B**) Morphology of muscle tissue in rats using H&E staining. (**C**) Western blot analysis of METTL3, METTL14, and WTAP expressions in rat muscle tissues. **P<0.01, ****P<0.0001. (**D**) IHC detection of METTL3 expression in rat muscle tissues. *P<0.05 vs the Sham group.

However, when METTL3 was knocked down, a decrease in ROS levels was observed (Figure 2H). These results imply that the NLRP3 inflammasome is activated and leads to cell pyroptosis in the case of ASTI and that METTL3 plays a role in mediating this process.

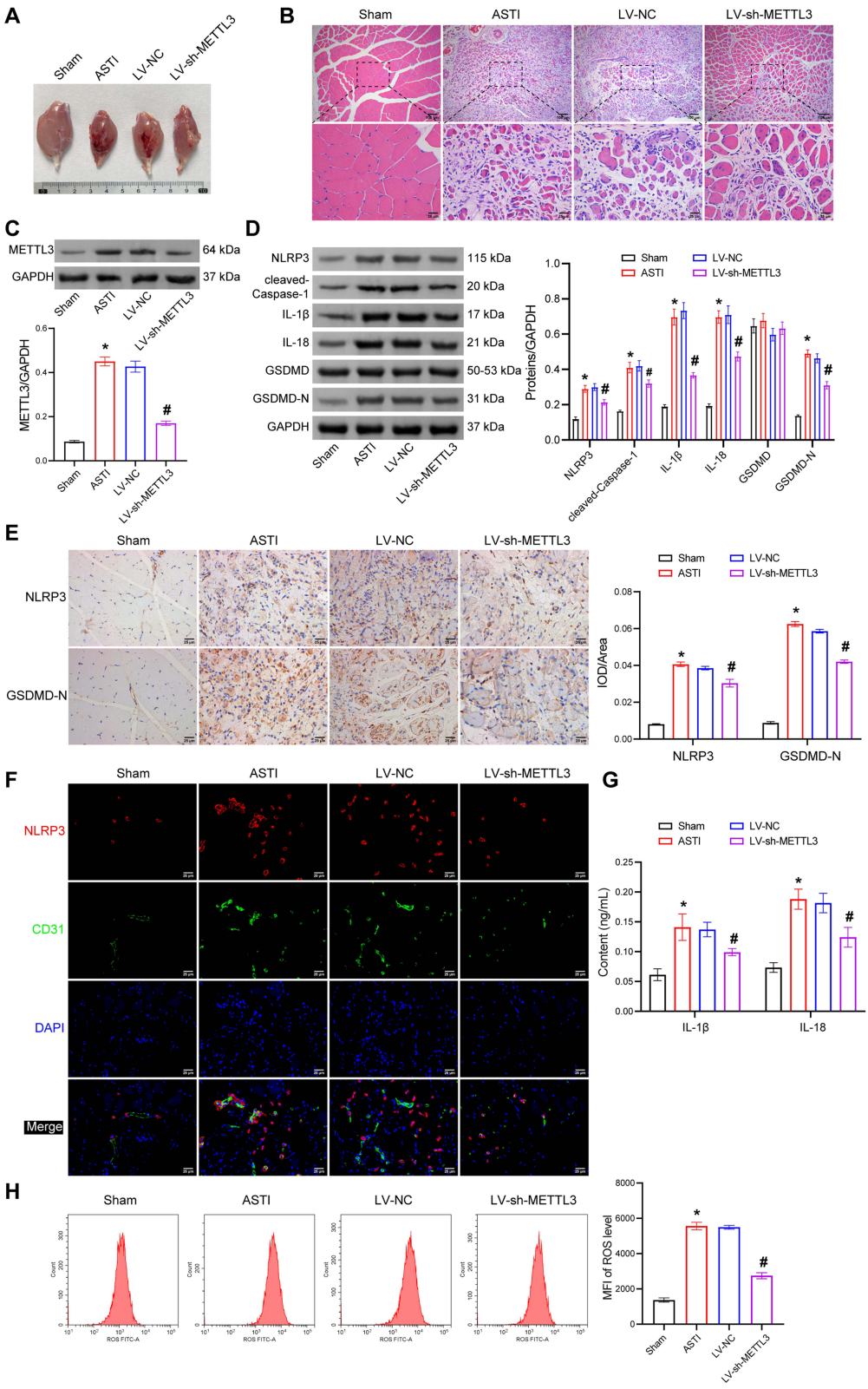

Figure 2 Modulation of METTL3 affects ASTI and cell pyroptosis in ASTI rats. (**A**) The images of the surface of muscle from rats. (**B**) Morphology of muscle tissue in rats using H&E staining. (**C**) Western blot analysis of METTL3 expression in rat muscle tissues. (**D**) Western blot analysis of pyroptosis-related protein expressions in rat muscle tissues. (**E**) IHC detection of METTL3 and GSDMD-N expression in rat muscle tissues. (**F**) IF detection of NLRP3 and CD31. (**G**) ELISA for IL-1β and IL-18 levels in rat muscle tissues. (**H**) Detection of ROS levels by flow cytometry. *P<0.05 vs the Sham group, #P<0.05 vs the LV-NC group.

Regulation of METTL3 Affects Endothelial Cell Pyroptosis

To further elucidate the relationship between METTL3 and cell pyroptosis, we established an LPS-ATP-induced in vitro injury model and constructed an in vitro model with low expression of METTL3. RT-qPCR and Western blot analysis verified successful METTL3 knockdown in HUVECs, and sh-METTL3-2 had the highest knockdown efficiency, which was used for subsequent experiments (Figure S1). In addition, Western blot analysis, it was determined that the expression of METTL3 was significantly higher in the cells of the Model group compared to the Control group. However, upon transfection with sh-METTL3, there was a notable decrease in the expression of METTL3 (Figure 3A). Furthermore, as depicted in Figure 3B, the Model group exhibited a significant increase in cell pyroptosis in contrast to the Control group. However, the knockdown of METTL3 effectively inhibited the LPS-ATP-induced cell pyroptosis. Subsequently, we investigated the impact of METTL3 on the protein levels of various pyroptosis-related markers. The presence of pyroptosis-related proteins was notably more prevalent in the Model group than in the Control group. Notably, the knockdown of METTL3 significantly suppressed LPS-ATP-induced pyroptosis-related protein levels (Figure 3C). The levels of IL-1β and IL-18 showed similar changes (Figure 3D). In addition, the results of the assay of cellular ROS levels showed that cellular ROS levels were elevated in the Model group compared with the Control group, and ROS levels decreased after the knockdown of METTL3 (Figure 3E). These results indicated that inhibition of METTL3 expression could alleviate LPS-ATP-induced endothelial cell pyroptosis.

METTL3 Promotes NLRP3 Expression by Regulating the m6A Modification Level of NLRP3

METTL3 is known to regulate NLRP3 mRNA m6A modification, which enhances ZBP1/NLRP3 protein interaction and promotes trophoblast cell pyroptosis.[17] Therefore, we validated the effect of METTL3 on m6A modification of NLRP3 in model cells. RNA m6A colorimetry results indicated that m6A levels were reduced in the sh-METTL3 group compared to the sh-NC group (Figure 4A). Moreover, the RIP assay analysis demonstrated that the knockdown of METTL3 resulted in a decrease in m6A levels of NLRP3 in HUVECs (Figure 4B). Furthermore, the results obtained from Western blot analyses provided compelling evidence, demonstrating a significant decrease in protein expression levels of NLRP3 in the sh-METTL3 group when compared to the sh-NC group (Figure 4C). These findings strongly suggest that METTL3 is involved in enhancing the m6A modification of NLRP3 and facilitating its expression in HUVECs.

Regulation of NLRP3 by m6A Modification Requires YTHDF1

The m6A-reader proteins are an integral part of the m6A modification process.[22] We found that YTHDF1, YTHDF2, YTHDF3, IGF2BP1, IGF2BP2, and IGF2BP3 could bind to NLRP3 by site prediction (http://rm2target.canceromics.org/#/home). To verify this result, we examined the protein levels of these m6A-reader proteins in rat muscle tissues and HUVECs, respectively. Western blot analysis of rat muscle tissues showed that the protein levels of YTHDF1, IGF2BP1, and IGF2BP3 were higher in the ASTI group than in the Sham group, with the most significant difference in YTHDF1 (Figure 5A). Western blot analysis of HUVECs showed that the protein levels of YTHDF1 and IGF2BP1 both had higher protein levels than the Control group, while the protein level of IGF2BP2 was lower than the Control group, with the most significant difference in YTHDF1 (Figure 5B). These results suggest that YTHDF1 may be associated with ASTI. Therefore, we further investigated the role of YTHDF1. RNA pulldown assay also confirmed that YTHDF1 could bind to NLRP3 mRNA (Figure 5C). Next, we constructed HUVECs with low expression of YTHDF1. RT-qPCR and Western blot analysis verified successful YTHDF1 knockdown in HUVECs, and sh-YTHDF1-3 had the highest knockdown efficiency, which was used for subsequent experiments (Figure 5D). Furthermore, as shown in Figure 5E and F, the knockdown of YTHDF1 decreased NLRP3 protein levels but did not affect mRNA levels in HUVEC compared with the sh-NC group. Overall, these results provide evidence suggesting that the m6A modification of NLRP3 is dependent on the participation of YTHDF1.

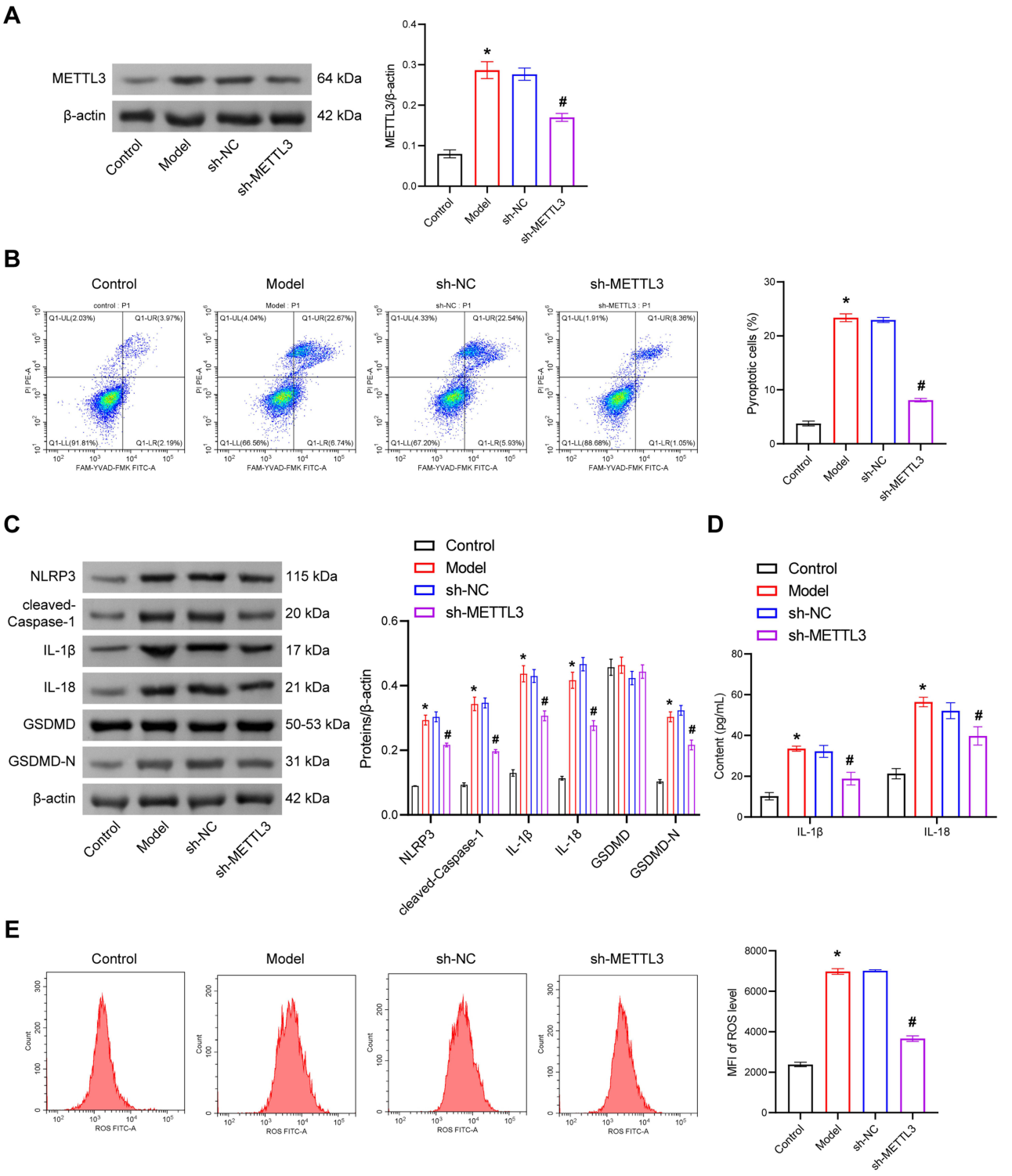

Figure 3 Regulation of METTL3 affects endothelial cell pyroptosis. (A) Western blot analysis of METTL3 expression in HUVECs. (**B**) Detection of cellular pyroptosis by flow cytometry. (**C**) Western blot analysis of pyroptosis-related protein expressions in HUVECs. (**D**) ELISA for IL-1β and IL-18 levels in HUVECs. (**E**) Detection of ROS levels by flow cytometry in HUVECs. *P<0.05 vs the Control group, #P<0.05 vs the sh-NC group.

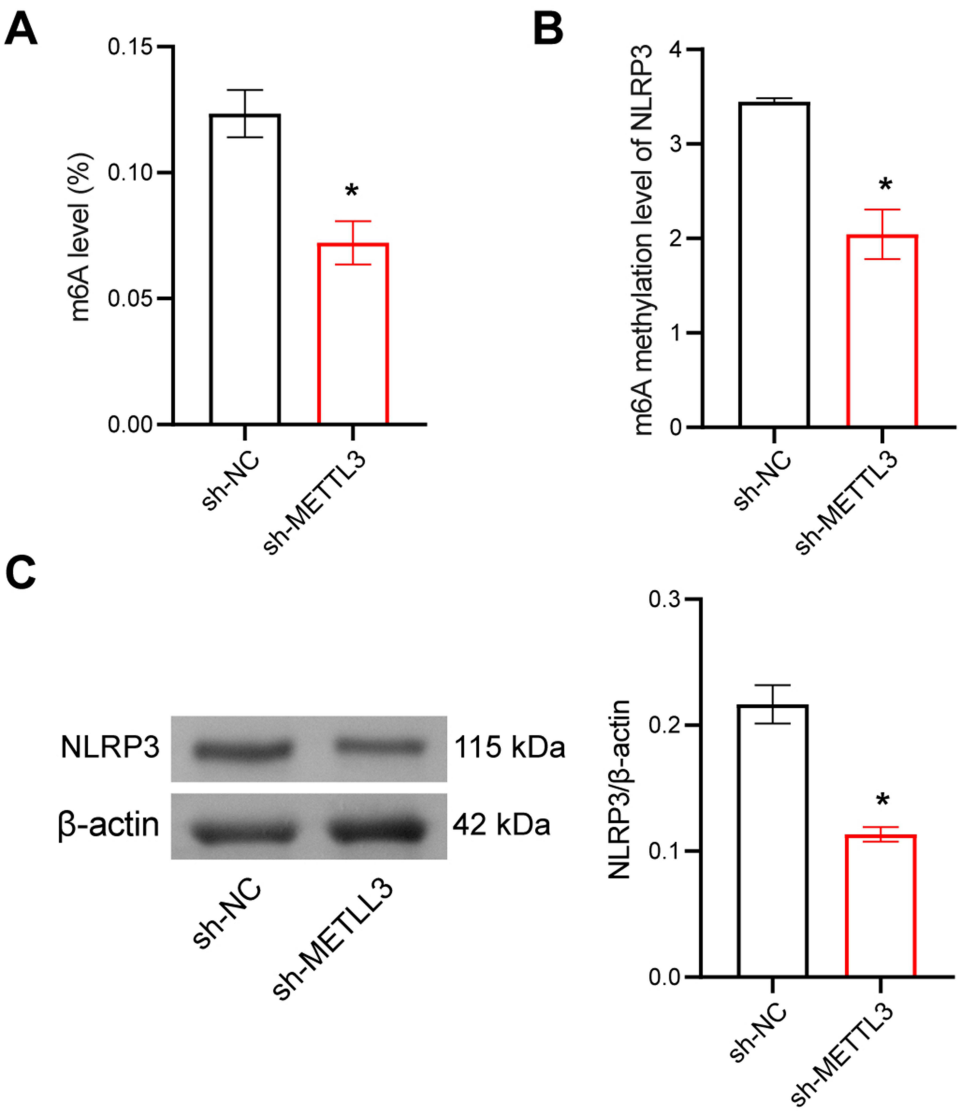

Figure 4 METTL3 promotes NLRP3 expression by regulating the m6A methylation level of NLRP3. (A) RNA m6A colorimetric assay was conducted to determine m6A levels in cells. (**B**) RIP assay was conducted to detect the m6A levels of NLRP3. (**C**) Western blot analysis of NLRP3 expression. *P<0.05 vs the sh-NC group.

Effect of Modulating NLRP3 to Reverse METTL3 on LPS-ATP-Induced Endothelial Cell Pyroptosis

To further investigate the potential mechanism of NLRP3 in the METTL3-mediated effect on LPS-ATP-induced endothelial cell pyroptosis, we cotransfected oe-NC or oe-NLRP3 and sh-METTL3 into LPS-ATP-induced HUVECs. Figure 6A showed that knockdown of METTL3 significantly inhibited LPS-ATP-induced cellular pyroptosis, which is consistent with the results in Figure 3B, and this inhibitory effect of sh-METTL3 was reversed after overexpression of NLRP3. In the sh-METTL3 group, the Western blot analysis revealed significantly reduced protein levels of NLRP3, cleaved-Caspase-1, IL-1β, IL-18, and GSDMD-N compared to the sh-NC group. Furthermore, overexpression of NLRP3 resulted in increased levels of these pyroptosis-related proteins (Figure 6B). The levels of IL-1β and IL-18 in cell supernatants showed similar changes (Figure 6C). In addition, the results of the detection of cellular ROS levels showed that cellular ROS levels were decreased in the sh-METTL3 group compared to the sh-NC group, and ROS levels were increased after overexpression of NLRP3 (Figure 6D). These findings suggest that NLRP3 mediates the impact of METTL3 on LPS-ATP-induced endothelial cell pyroptosis.

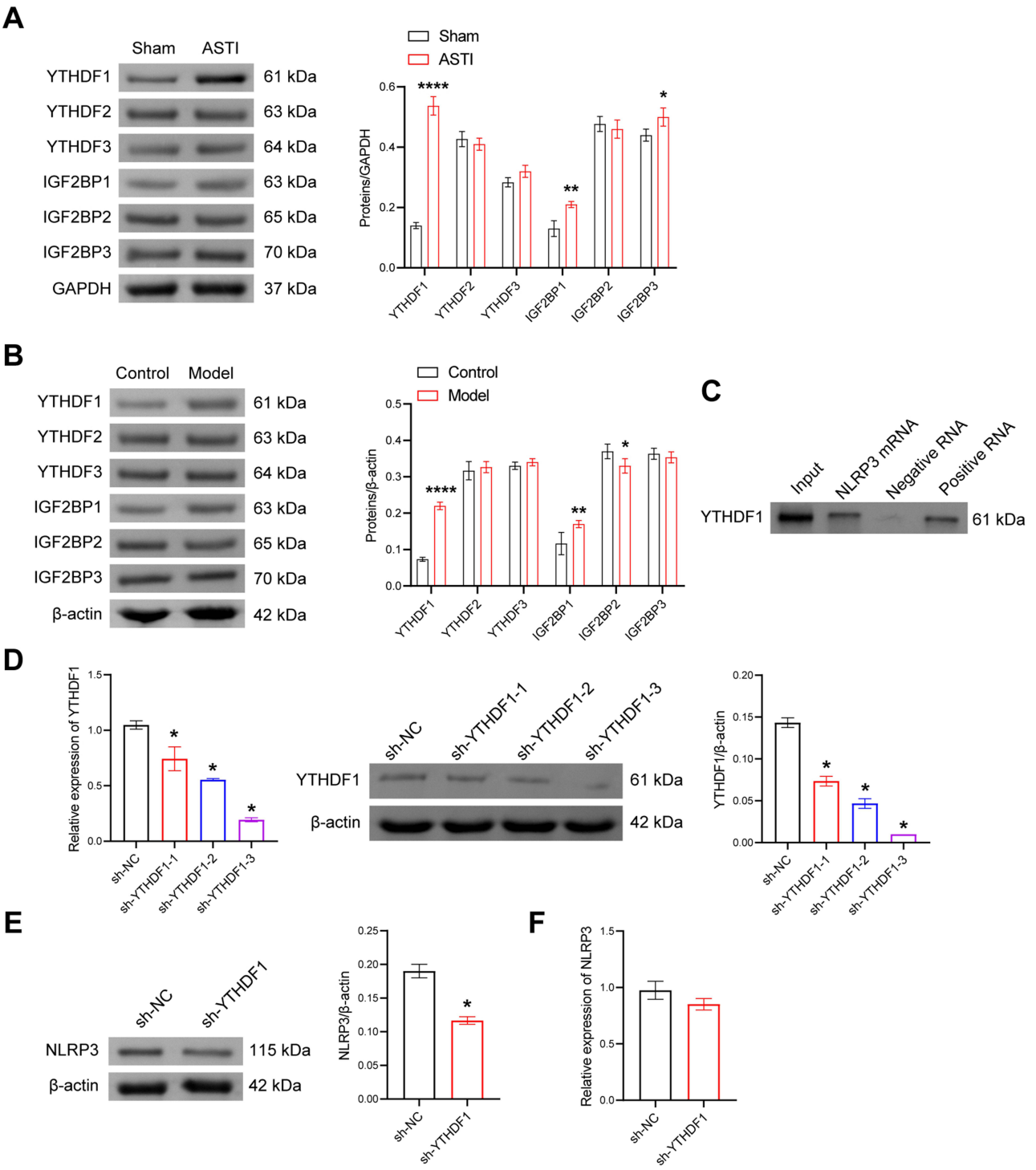

Figure 5 Regulation of NLRP3 by m6A methylation requires YTHDF1. (**A** and **B**) Western blot analysis of YTHDF1, YTHDF2, YTHDF3, IGF2BP1, IGF2BP2, and IGF2BP3 expressions in rat muscle tissues and HUVECs. *P<0.05, **P<0.01, ****P<0.0001. (**C**) RNA pulldown assay was performed to evaluate the interaction between NLRP3 and YTHDF1. (**D**) RT-qPCR and Western blot analysis of YTHDF1 expression in HUVECs. (**E**) Western blot analysis of NLRP3 expression in HUVECs. (**F**) RT-qPCR assay for detecting NLRP3 mRNA levels in HUVECs. *P<0.05 vs the sh-NC group.

Discussion

ASTI is characterized by skeletal muscle damage, which includes local tissue necrosis, capillary dilation, tissue edema, inflammatory cell infiltration, and release.[23] In addition to causing damage to muscle cells, this process also interferes with the normal functioning of endothelial cells. The disruption of endothelial cell function is known to be critically

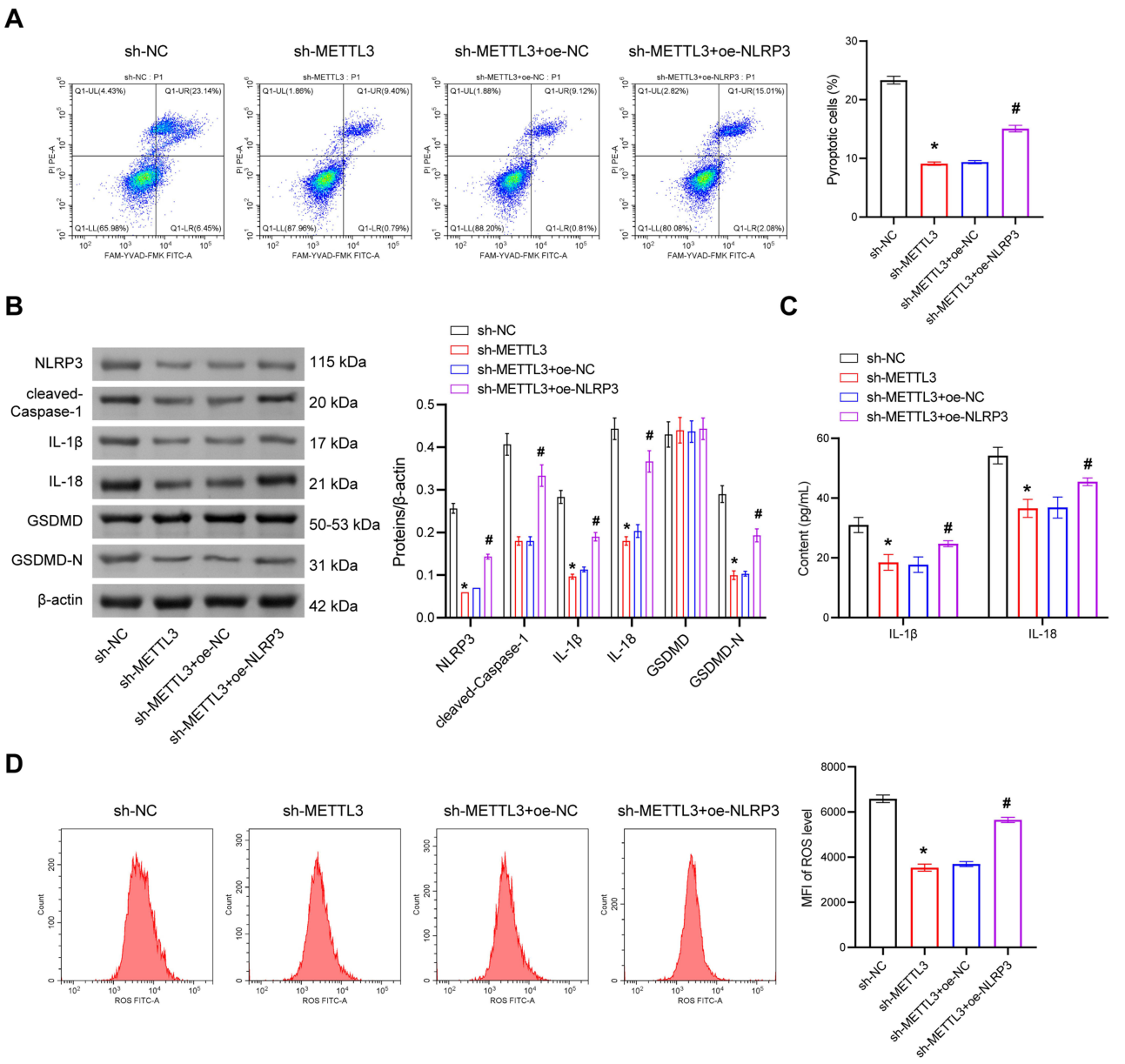

Figure 6 Regulation of METTL3 affects LPS-ATP-induced endothelial cell pyroptosis. (A) Detection of cellular pyroptosis by flow cytometry. (**B**) Western blot analysis of pyroptosis-related protein expressions in HUVECs. (**C**) ELISA for IL-1β and IL-18 levels in HUVECs. (**D**) Detection of ROS levels by flow cytometry in HUVECs. *P<0.05 vs the sh-NC group, #P<0.05 vs the sh-METTL3+oe-NC group.

involved in the initiation and progression of ASTI.[4,5] As a protective response after muscle tissue damaged, inflammation is very common.[24] Previous studies have shown the presence of leukocyte infiltration and local inflammation in damaged tissues, with overexpression of pro-inflammatory cytokines.[25,26] The inflammatory cytokines primarily responsible for regulating the cellular environment and influencing the progression of other repair mechanisms.[26] It is therefore essential to target inflammation when developing treatments aimed at facilitating faster recovery. Pyroptosis, a pro-inflammatory form of programmed cell death triggered by the NLRP3 inflammasome and dependent on Caspase-1 activation, has been identified as a potential mechanism to target in this regard.[27]

Previous research has highlighted the significant role of endothelial cell pyroptosis in the process of wound healing.[12] The pathophysiological mechanisms of ASTI are similar to those of wound injury. Furthermore, the activation of the NLRP3 inflammasome and the resulting pyroptosis have also been implicated in the mechanism underlying the cadmium-induced inflammatory response in HUVECs.[28] Hence, it can be inferred that endothelial cell pyroptosis

might play a crucial role in the progression of ASTI. Our study confirmed this, as increased expression of pyroptosis-related proteins was detected in both the ASTI rat model and the LPS-ATP induced in vitro injury model. In addition, levels of the inflammatory cytokines IL-1β and IL-18, and ROS were elevated, indicating an increased level of NLRP3 inflammasome-mediated cell pyroptosis in ASTI. However, when METTL3 was knocked down, the level of cell pyroptosis decreased, and ASTI was alleviated.

m6A, formed by RNA methylation in mRNA, is the most prevalent internal modification and plays a vital role in multiple molecular and cellular processes.[29,30] m6A is a reversible RNA modification that occurs through methylation by methyltransferases (writers) and can be demethylated by demethylases (erasers). Following m6A modification of RNA bases, specific enzymes known as "readers" recognize these modified sites, subsequently influencing processes such as RNA translation, decay, and stability downstream.[30] Furthermore, it regulates cell fate determination, cell cycle arrest, and cell differentiation, and ultimately contributes to the development of various diseases.[31] Members of the m6A "writers" include METTL3, METTL14, and WTAP, with METTL3 being primarily responsible for synthesizing nearly all m6A in the mRNA transcriptome.[32] However, there have been no reports on m6A methylation in ASTI so far. In our study, we measured the expression of these three m6A "writers" in injured muscle tissue from the ASTI rat model for the first time. According to the Western blot analysis, METTL3, METTL14, and WTAP protein expression levels were found to be elevated in the ASTI rats compared to the Control group. Specifically, METTL3 exhibited the most significant difference in expression between the two groups. IHC results also indicated a high expression of METTL3 in ASTI. Previous studies have shown that METTL3 enhances VEGF3-mediated lymphangiogenesis through the regulation of VEGF-C m6A modification in ADSCs, promoting wound healing.[16] In our further investigation of the role of METTL3 in ASTI, we knocked down METTL3 in the ASTI rats and observed reduced tissue damage and weakened inflammatory response, suggesting that inhibiting METTL3 can alleviate ASTI.

Emerging evidence suggests that m6A plays a key role in the regulation of cell pyroptosis pathways.[33,34] Moreover, METTL3 enhances cell pyroptosis by increasing m6A methylation on NLRP3 mRNA and its stability, thereby promoting the interaction between ZBP1 and NLRP3 protein.[17] Similarly, we also found that inhibiting METTL3 can alleviate cell pyroptosis in both in vivo and in vitro models of ASTI. To further investigate the role of METTL3 in NLRP3 mRNA m6A methylation, we conducted RIP, PCR, and Western blot assays and found that knocking down METTL3 resulted in decreased m6A levels on NLRP3 mRNA, leading to reduced expression of NLRP3. Moreover, overexpression of NLRP3 reversed the inhibitory effect of METTL3 knockdown on HUVECs cell pyroptosis. These findings suggest that METTL3 promotes HUVEC cell pyroptosis by increasing m6A methylation on NLRP3 mRNA and NLRP3 expression. However, it has also been reported that METTL3 can alleviate high glucose-induced retinal pigment epithelium (RPE) cell pyroptosis, and this effect is mediated by targeting the miR-25-3p/PTEN/AKT signaling.[35] This discrepancy may be due to the different downstream target genes regulated by METTL3 in different cell types.

During the m6A modification process, the involvement of m6A "readers" is also required. METTL3, by affecting the m6A levels on mRNA, alters the recognition capability of m6A readers towards mRNA molecules, consequently influencing gene expression.[36] The YTH domain-containing family was initially identified as m6A reader proteins, including YTHDF1, YTHDF2, and YTHDF3.[37] YTHDF1 has been shown to enhance the translation of NLRP3 and promote inflammation in a mouse model of sepsis.[38] However, the interaction between YTHDF1 and NLRP3 in ASTI has not been reported yet. In our study, we first predicted potential m6A readers that may interact with NLRP3 using bioinformatic analysis. Subsequently, we examined the expression of RNA m6A reader proteins, including YTHDF1, YTHDF2, YTHDF3, IGF2BP1, IGF2BP2, and IGF2BP3, in both in vivo and in vitro models of ASTI using Western blot. The results showed that YTHDF1 was highly expressed in both in vivo and in vitro models of ASTI, and it interacted with NLRP3 mRNA. Furthermore, Western blot and RT-qPCR assays showed that the knockdown of YTHDF1 decreased NLRP3 protein expression in HUVECs but did not affect NLRP3 mRNA levels. These findings suggest that YTHDF1 binds to NLRP3 mRNA and regulates NLRP3 expression by promoting its translation.

Limitation

In our study, we simulated an ASTI animal model through impact experiments. However, others have utilized clamp compression on thigh muscles to mimic the ASTI animal model in different research.[39] Whether our study's conclusions are applicable to these other models remains uncertain. Therefore, further research is necessary to validate these findings. Additionally, further validation in clinical samples to assess its clinical feasibility represents a future research direction for us.

Conclusions

The main findings of this study demonstrate that METTL3 mediates endothelial cell pyroptosis in soft tissue injury by increasing m6A methylation and enhancing NLRP3 expression, and this effect also requires the involvement of m6A reader protein YTHDF1. This discovery may provide new directions for the treatment of ASTI.

Abbreviations

ASTI, Acute soft tissue injury; ECM, endothelial cell medium; GSDMD-N, N-terminal fragment of GSDMD; HUVECs, Human umbilical vein endothelial cells; IHC, Immunohistochemistry; IF, Immunofluorescence; METTL3, Methyltransferase-like 3; LPS, Lipopolysaccharide; m6A, N6-methyladenosine; NLRP3, NOD-like receptor protein 3; RPE, retinal pigment epithelium.

Data Sharing Statement

Data will be made available on request.

Ethics Approval Statement

This study was carried out in accordance with the recommendations of Experimental Animals Welfare Guideline of Xiangtan Central Hospital Animal Care and Research Committee. The protocol was approved by the Animal Ethics Committee of Xiangtan Central Hospital.

Author Contributions

All authors made a significant contribution to the work reported, whether that is in the conception, study design, execution, acquisition of data, analysis and interpretation, or in all these areas; took part in drafting, revising or critically reviewing the article; gave final approval of the version to be published; have agreed on the journal to which the article has been submitted; and agree to be accountable for all aspects of the work.

Disclosure

The authors declare that they have no competing interests in this work.

References

1. Frick MA, Murthy NS. Imaging of the elbow: muscle and tendon injuries. *Semin Musculoskelet Radiol*. 2010;14(4):430–437. doi:10.1055/s-0030-1263258
2. Bleakley C, McDonough S, MacAuley D. The use of ice in the treatment of acute soft-tissue injury: a systematic review of randomized controlled trials. *Am J Sports Med*. 2004;32(1):251–261. doi:10.1177/0363546503260757
3. George C, Smith C, Isaacs A, et al. Chronic Prosopis glandulosa treatment blunts neutrophil infiltration and enhances muscle repair after contusion injury. *Nutrients*. 2015;7(2):815–830. doi:10.3390/nu7020815
4. Amarasekera AT, Chang D, Schwarz P, et al. Does vascular endothelial dysfunction play a role in physical frailty and sarcopenia? A systematic review. *Age Ageing*. 2021;50(3):725–732. doi:10.1093/ageing/afaa237
5. Liu X, Sun X, Liao H, et al. Mitochondrial aldehyde dehydrogenase 2 regulates revascularization in chronic ischemia: potential impact on the development of coronary collateral circulation. *Arterioscler Thromb Vasc Biol*. 2015;35(10):2196–2206. doi:10.1161/ATVBAHA.115.306012
6. Ding J, Li F, Cong Y, et al. Trichostatin A inhibits skeletal muscle atrophy induced by cigarette smoke exposure in mice. *Life Sci*. 2019;235:116800. doi:10.1016/j.lfs.2019.116800
7. Martinon F, Burns K, Tschopp J. The inflammasome: a molecular platform triggering activation of inflammatory caspases and processing of proIL-beta. *Mol Cell*. 2002;10(2):417–426. doi:10.1016/S1097-2765(02)00599-3

8. Lei Y, Xu T, Sun W, et al. Evodiamine alleviates DEHP-induced hepatocyte pyroptosis, necroptosis and immunosuppression in grass carp through ROS-regulated TLR4 / MyD88 / NF-κB pathway. *Fish Shellfish Immunol*. 2023;140:108995. doi:10.1016/j.fsi.2023.108995
9. Shi J, Zhao Y, Wang K, et al. Cleavage of GSDMD by inflammatory caspases determines pyroptotic cell death. *Nature*. 2015;526(75):660–665.
10. Lv X, Ren M, Xu T, et al. Selenium alleviates lead-induced CIK cells pyroptosis and inflammation through IRAK1/TAK1/IKK pathway. *Fish Shellfish Immunol*. 2023;142:109101. doi:10.1016/j.fsi.2023.109101
11. Loveless R, Bloomquist R, Teng Y. Pyroptosis at the forefront of anticancer immunity. *J Exp Clin Cancer Res*. 2021;40(1):264. doi:10.1186/s13046-021-02065-8
12. Zhang K, Chai B, Ji H, et al. Bioglass promotes wound healing by inhibiting endothelial cell pyroptosis through regulation of the connexin 43/reactive oxygen species (ROS) signaling pathway. *Lab Invest*. 2022;102(1):90–101. doi:10.1038/s41374-021-00675-6
13. Lin S, Choe J, Du P, et al. The m(6)A methyltransferase METTL3 promotes translation in human cancer cells. *Mol Cell*. 2016;62(3):335–345. doi:10.1016/j.molcel.2016.03.021
14. Yang L, Ren Z, Yan S, et al. Nsun4 and Mettl3 mediated translational reprogramming of Sox9 promotes BMSC chondrogenic differentiation. *Commun Biol*. 2022;5(1):495. doi:10.1038/s42003-022-03420-x
15. Luo X, Zhu S, Li J, et al. Potential genetic therapies based on m6A methylation for skin regeneration: wound healing and scars/keloids. *Front Bioeng Biotechnol*. 2023;11:1143866. doi:10.3389/fbioe.2023.1143866
16. Zhou J, Wei T, He Z. ADSCs enhance VEGFR3-mediated lymphangiogenesis via METTL3-mediated VEGF-C m(6)A modification to improve wound healing of diabetic foot ulcers. *Mol Med*. 2021;27(1):146. doi:10.1186/s10020-021-00406-z
17. Wang R, Xu X, Yang J, et al. BPDE exposure promotes trophoblast cell pyroptosis and induces miscarriage by up-regulating lnc-HZ14/ZBP1/NLRP3 axis. *J Hazard Mater*. 2023;455:131543. doi:10.1016/j.jhazmat.2023.131543
18. Yang H, Zhou J, Pan H, et al. Mesenchymal stem cells derived-exosomes as a new therapeutic strategy for acute soft tissue injury. *Cell Biochem Funct*. 2021;39(1):107–115. doi:10.1002/cbf.3570
19. Qian H, Deng X, Huang Z-W, et al. An HNF1α-regulated feedback circuit modulates hepatic fibrogenesis via the crosstalk between hepatocytes and hepatic stellate cells. *Cell Res*. 2015;25(8):930–945. doi:10.1038/cr.2015.84
20. Tong J, Flavell RA, Li HB. RNA m(6)A modification and its function in diseases. *Front Med*. 2018;12(4):481–489. doi:10.1007/s11684-018-0654-8
21. Abais JM, Xia M, Zhang Y, et al. Redox regulation of NLRP3 inflammasomes: ROS as trigger or effector? *Antioxid Redox Signal*. 2015;22(13):1111–1129. doi:10.1089/ars.2014.5994
22. Liu T, Wei Q, Jin J, et al. The m6A reader YTHDF1 promotes ovarian cancer progression via augmenting EIF3C translation. *Nucleic Acids Res*. 2020;48(7):3816–3831. doi:10.1093/nar/gkaa048
23. Tidball JG. Mechanisms of muscle injury, repair, and regeneration. *Compr Physiol*. 2011;1(4):2029–2062.
24. Yin K, Wang D, Zhang Y, et al. Polystyrene microplastics promote liver inflammation by inducing the formation of macrophages extracellular traps. *J Hazard Mater*. 2023;452:131236. doi:10.1016/j.jhazmat.2023.131236
25. Wang S, Li T, Qu W, et al. The effects of xiangqing anodyne spray on treating acute soft-tissue injury mainly depend on suppressing activations of AKT and p38 pathways. *Evid Based Complement Alternat Med*. 2016;2016:9213489. doi:10.1155/2016/9213489
26. Tidball JG. Inflammatory processes in muscle injury and repair. *Am J Physiol Regul Integr Comp Physiol*. 2005;288(2):R345–R353. doi:10.1152/ajpregu.00454.2004
27. LaRock CN, Cookson BT. Burning down the house: cellular actions during pyroptosis. *PLoS Pathog*. 2013;9(12):e1003793. doi:10.1371/journal.ppat.1003793
28. Chen H, Lu Y, Cao Z, et al. Cadmium induces NLRP3 inflammasome-dependent pyroptosis in vascular endothelial cells. *Toxicol Lett*. 2016;246:7–16. doi:10.1016/j.toxlet.2016.01.014
29. Shi H, Wei J, He C. Where, when, and how: context-dependent functions of RNA methylation writers, readers, and erasers. *Mol Cell*. 2019;74(4):640–650. doi:10.1016/j.molcel.2019.04.025
30. Zaccara S, Ries RJ, Jaffrey SR. Reading, writing and erasing mRNA methylation. *Nat Rev Mol Cell Biol*. 2019;20(10):608–624. doi:10.1038/s41580-019-0168-5
31. Wu Y, Zhou C, Yuan Q. Role of DNA and RNA N6-adenine methylation in regulating stem cell fate. *Curr Stem Cell Res Ther*. 2018;13(1):31–38. doi:10.2174/1574888X12666170621125457
32. Bokar JA, Shambaugh ME, Polayes D, et al. Purification and cDNA cloning of the adomet-binding subunit of the human mRNA (N6-adenosine)-methyltransferase. *Rna*. 1997;3(11):1233–1247.
33. Zhang L, Hou C, Chen C, et al. The role of N(6)-methyladenosine (m(6)A) modification in the regulation of circRNAs. *Mol Cancer*. 2020;19(1):105. doi:10.1186/s12943-020-01224-3
34. Liu BH, Tu Y, Ni G-X, et al. Total flavones of abelmoschus manihot ameliorates podocyte pyroptosis and injury in high glucose conditions by targeting METTL3-dependent m(6)a modification-mediated NLRP3-inflammasome activation and PTEN/PI3K/Akt signaling. *Front Pharmacol*. 2021;12:667644. doi:10.3389/fphar.2021.667644
35. Zha X, Xi X, Fan X, et al. Overexpression of METTL3 attenuates high-glucose induced RPE cell pyroptosis by regulating miR-25-3p/PTEN/Akt signaling cascade through DGCR8. *Aging*. 2020;12(9):8137–8150. doi:10.18632/aging.103130
36. Song H, Feng X, Zhang H, et al. METTL3 and ALKBH5 oppositely regulate m A modification of TFE mRNA, which dictates the fate of hypoxia/reoxygenation-treated cardiomyocytes. *Autophagy*. 2019;15(8):1419–1437. doi:10.1080/15548627.2019.1586246
37. Sikorski V, Selberg S, Lalowski M, et al. The structure and function of YTHDF epitranscriptomic m(6)A readers. *Trends Pharmacol Sci*. 2023;44(6):335–353. doi:10.1016/j.tips.2023.03.004
38. Hao WY, Lou Y, Hu G-Y, et al. RNA m6A reader YTHDF1 facilitates inflammation via enhancing NLRP3 translation. *Biochem Biophys Res Commun*. 2022;616:76–81. doi:10.1016/j.bbrc.2022.05.076
39. Kobbe P, Kaczorowski DJ, Vodovotz Y, et al. Local exposure of bone components to injured soft tissue induces toll-like receptor 4-dependent systemic inflammation with acute lung injury. *Shock*. 2008;30(6):686–691. doi:10.1097/SHK.0b013e31816f257e